Improvement of Sonodynamic Cancer Therapy by Porphyrin-Based Sonosensitizer

Literature Seminar

2022/1/28

Keiichi Kawabata (M1)

Contents

Contents

Photodynamic Therapy (PDT) and Sonodynamic Therapy (SDT)

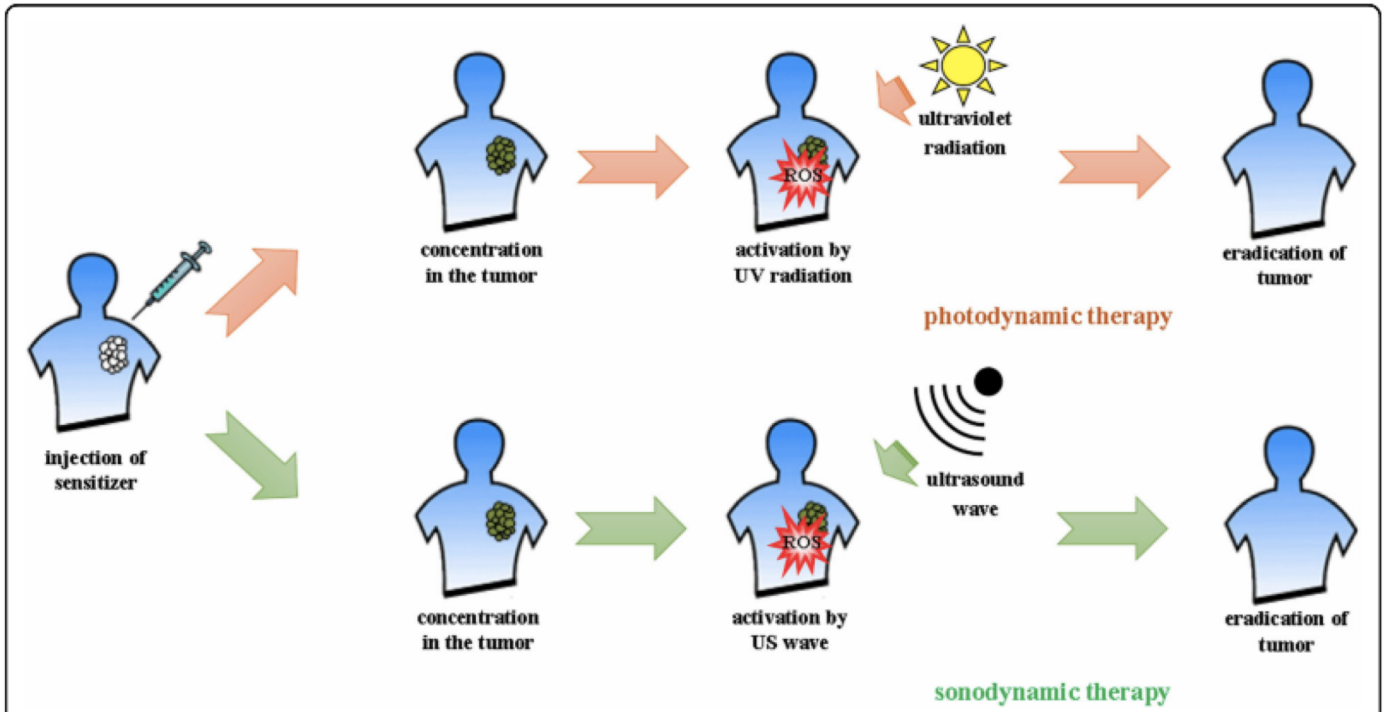

Fig. 2 Milestones of photodynamic therapy (PDT) and sonodynamic therapy (SDT) in tumor treatment. Cancer therapies, such as PDT or SDT, build on the administration of sensitive agents into tumor, followed by their activation by UV radiation or US wave, respectively. Activated photo- or sonosensitizers generate ROS that lead to cancer cell eradication

Bogdan, *et al., Nanoscale Res. Lett.*, **2017**, *12*, 225

Merits of SDT

- Non-invasive
- More penetrative than PDT

Cavitation

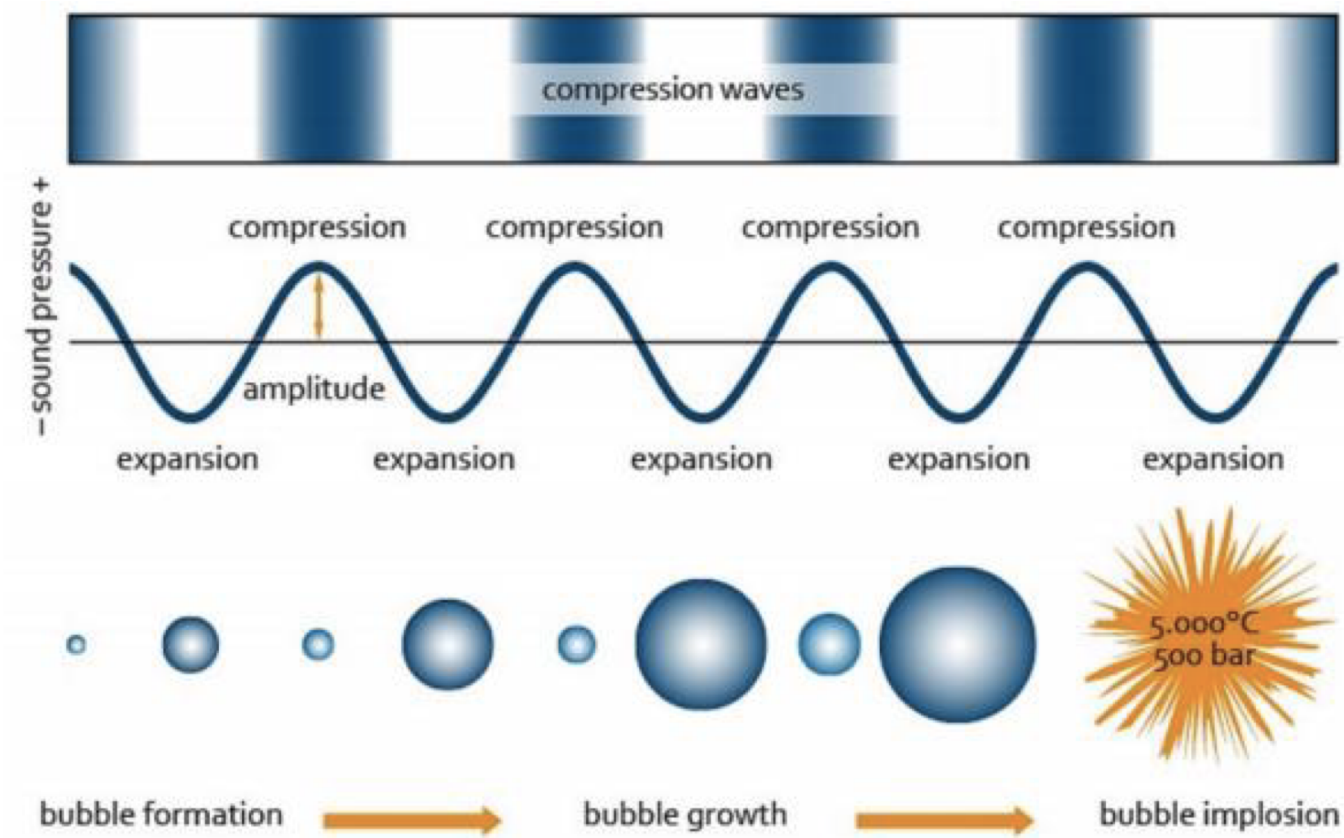

Figure 1. Principle of ultrasound cavitation [16]. The initiated bubbles grow due to evaporation and finally reach critical size (resonant) when it grows quickly and collapse violently.

J, Ö., *et al., Sustainable and energy efficient leaching of tungsten (W) by ultrasound controlled cavitation,* **2017**, p8

Mechanism of SDT

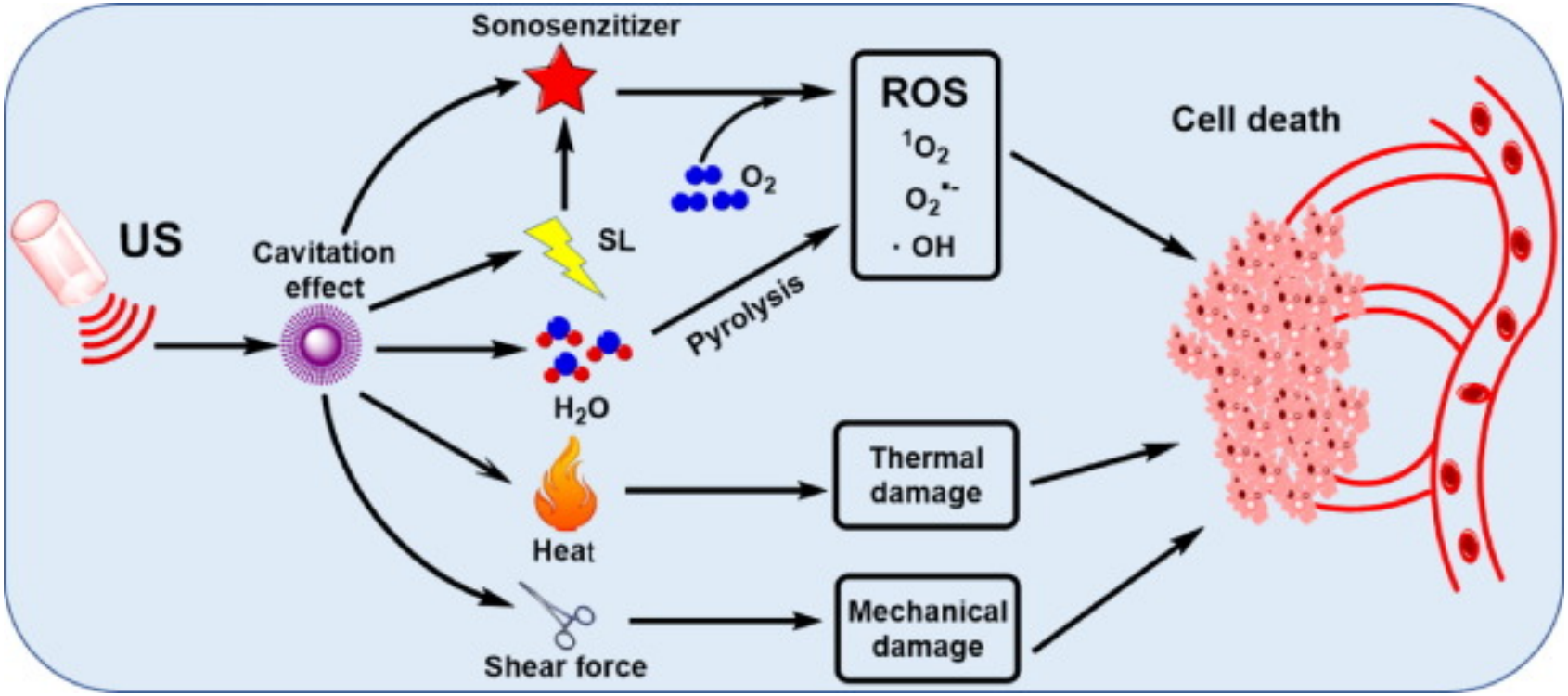

Xing, X. *et al., Coordination Chemistry Reviews*, **2021**, *445*, 214087

Generation of $^1O_2$

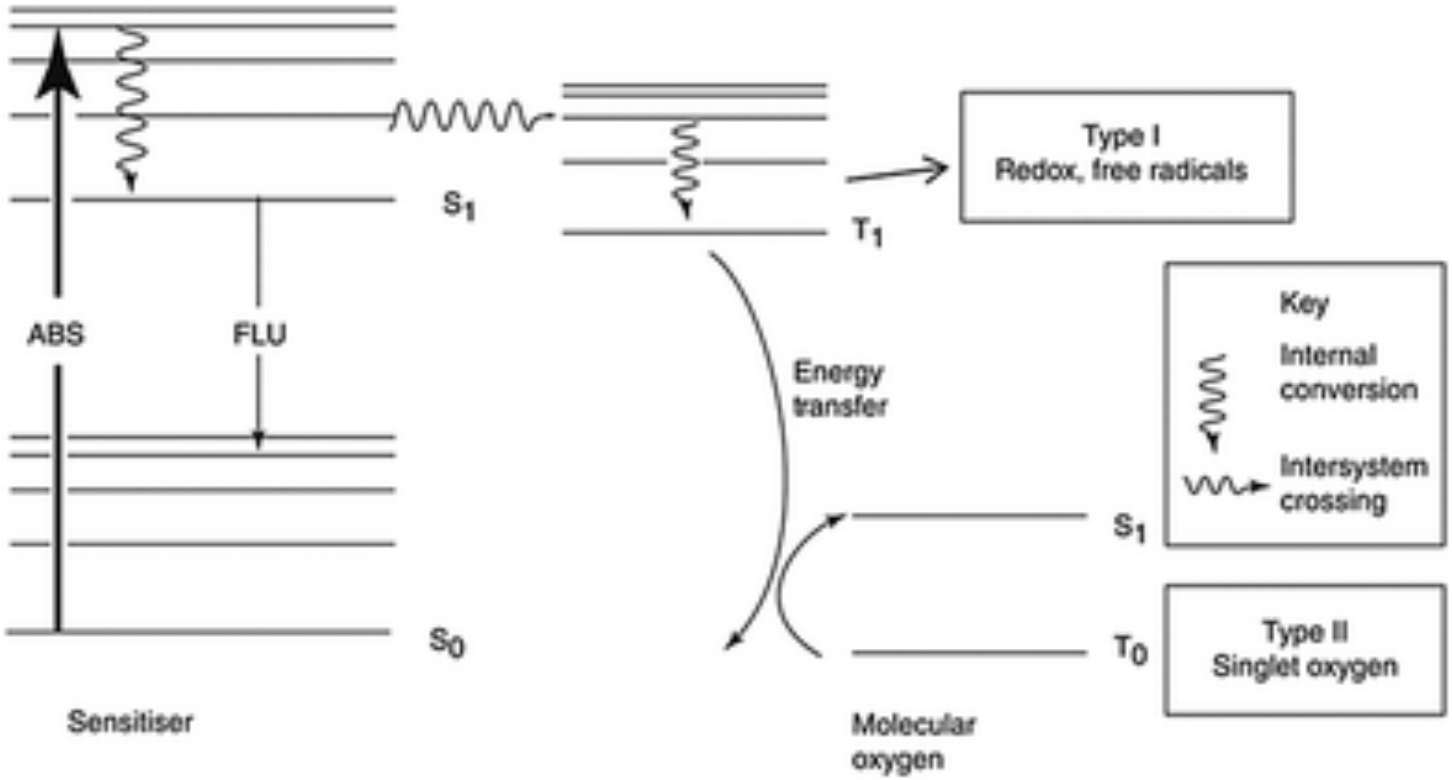

McHale, A. P. *et al., Therapeutic Ultrasound*, **2016**, *880*, 429–450

Organic Sonosensitizers

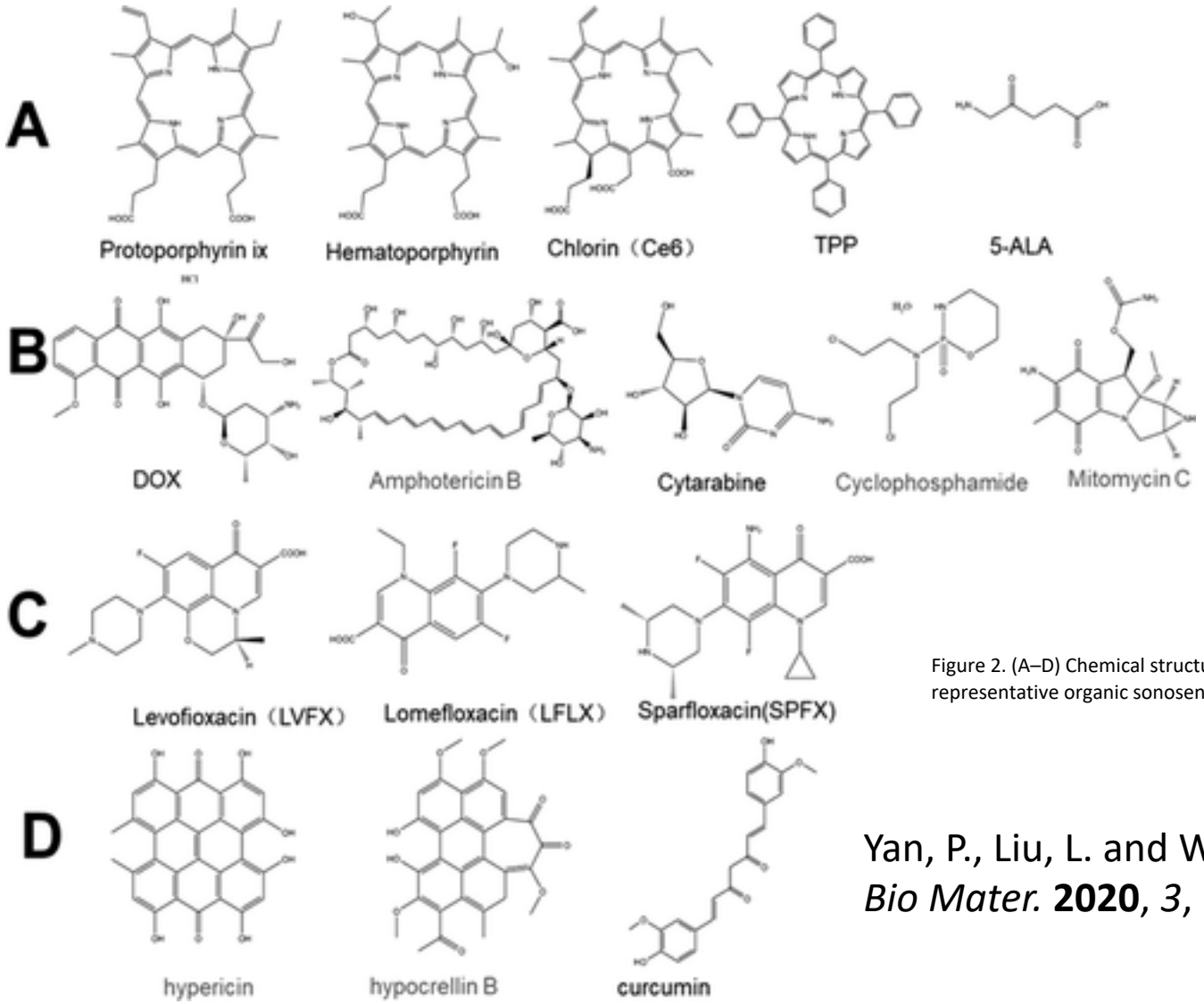

Figure 2. (A–D) Chemical structures of representative organic sonosensitizers.

Yan, P., Liu, L. and Wang, P., *ACS Appl. Bio Mater.* **2020**, *3*, 6, 3456–3475

Porphyrins

- Most widely used sonosensitizer
- Large π-electron conjugated system
- Various metals at center

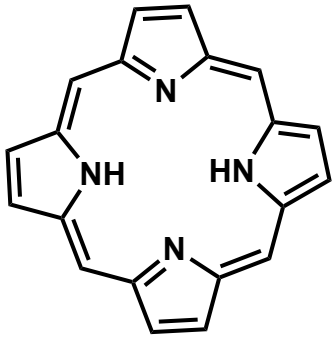

Improvement points

- Demerits of organic sonosensitizers
  - Phototoxicity
  - Low water solubility
  - Deficiency of targeting ability
  - Fast metabolism
- A good sonosensitizer should
  - be of high sonosensitivity
  - be non-toxic in the absence of ultrasound
  - specifically accumulate in the target
  - be excreted from the body within a proper period

Contents

MTTP-HSA Nanocomplex

- Metal-porphyrin complexes were encapsulated by HSA (human serum albumin)
  - →solve, reduce toxicity, prolong circulation time, enhance effect
- Red shift of Soret band

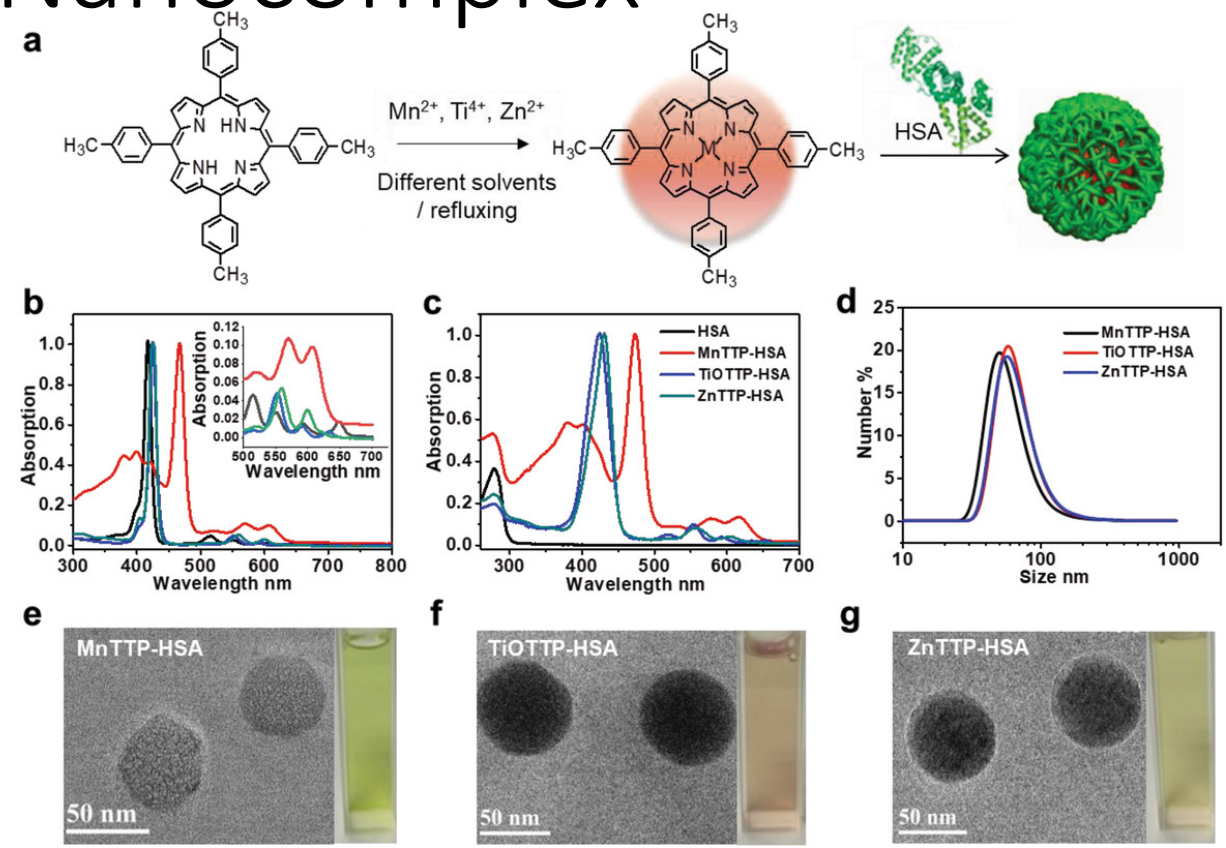

Figure1
Schematic illustration and characterization of MTTP complexes and MTTP-HSA nanocomplexes. a) A scheme illustrating the synthesis of MTTP complexes and the corresponding nanocomplexes of HSA. b) UV–vis absorption spectra of TTP and the three metal-porphyrin coordination complexes in DMF; the inset is the Q-band absorption of TTP and its metal complexes. c) UV–vis spectra of the three MTTP-HSA nanocomplexes in water; the absorption peak at 280 nm belongs to HSA. d) The size distribution of MTTP-HSA nanocomplexes, with the average diameter of about 60 nm. e–g) TEM images of MTTP-HSA nanocomplexes, showing spherical structures; the insets show the colors of the three nanocomplex solutions (5.5×10^{-6} m in water), influenced by their metal centers.

Ma, A. *et al.*, *Small*, **2019**, *15*, e1804028

$^1O_2$ Generation by MTTP-HSA

- MTTP-HSA generated not radicals but $^1O_2$
- MTTP-HSA generated $^1O_2$ up to 11 cm away from the US probe
- MnTTP had the best activity of the three

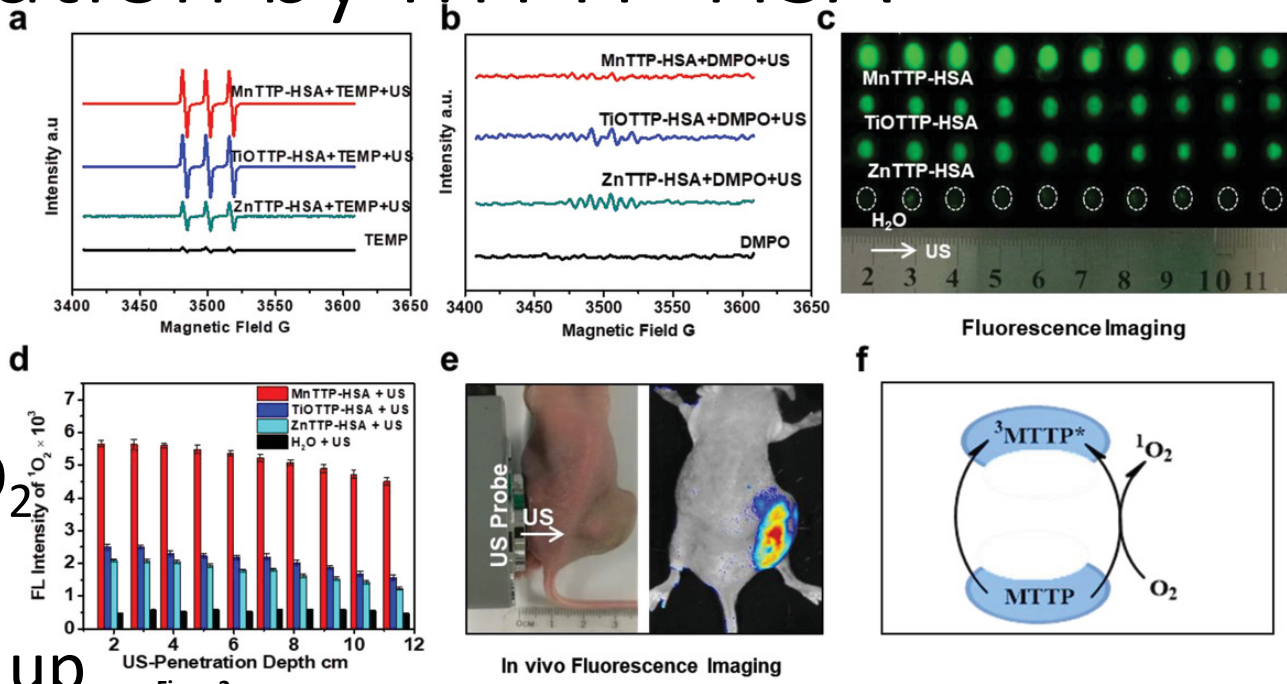

Figure2

$^1O_2$ generation and the SDT effects of MTTP-HSAs irradiated by US treatment (1 MHz, 2 W cm^{-2}, 50% duty cycle). a) ESR spectra for detecting $^1O_2$ generation from these nanocomplexes after US treatment; 2,2,6,6-tetramethylpiperidine (TEMP) without US irradiation was used as a control for comparison. Singlet oxygen was significantly observed. b) ESR spectra for detecting radical generation from these nanocomplexes after US treatment; 5,5-dimethyl-1-pyrroline-N-oxide (DMPO) without US irradiation was used as a control for comparison. No obvious radical species were clearly generated. c) The FL imaging for the detection for depth-activated $^1O_2$ generation under US irradiation in mimic tissue using SOSG as $^1O_2$ probe. Measurements were made at depth up to 11 cm. d) $^1O_2$ quantitative measurement of depth-dependent FL intensity of these nanocomplexes after US irradiation. e) Photographs of the US treatment method and in vivo ROS fluorescent images after 5 min of US treatment with the injection of MnTTP-HSA nanoparticles. f) The diagram illustrating the possible US-excitation transfer between a metalloporphyrin complexes and oxygen molecule

Ma, A. *et al.*, *Small*, **2019**, *15*, e1804028

HOMO-LUMO plots of MTTP

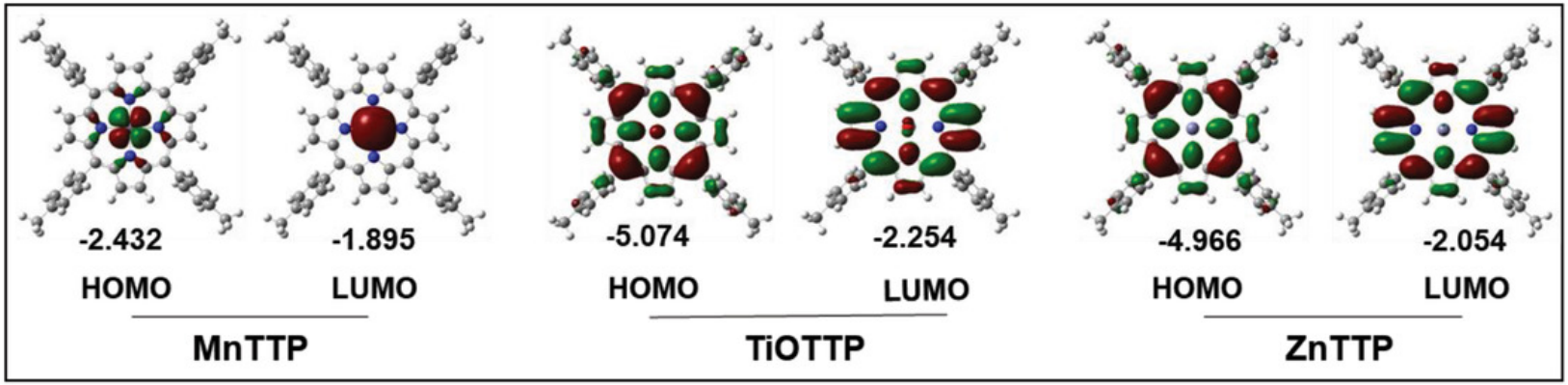

Figure2
g) HOMO-LUMO plots of these simulated complexes by density functional theory (the orbital energies presented in eV).

- HOMO/LUMO of MnTTP are strongly localized on Mn^{2+}
- HOMO/LUMO of TiOTTP/ZnTTP are mainly delocalized on the p AOs of C/N atoms on the porphyrin
- Energy gap of MnTTP was lower than that of TiOTTP/ZnTTP
  - →can be irradiated by low intensity
  - →stronger ability of $^1O_2$ generation

Ma, A. *et al.*, *Small*, **2019**, *15*, e1804028

In Vivo SDT Efficiency of MnTTP-HSA

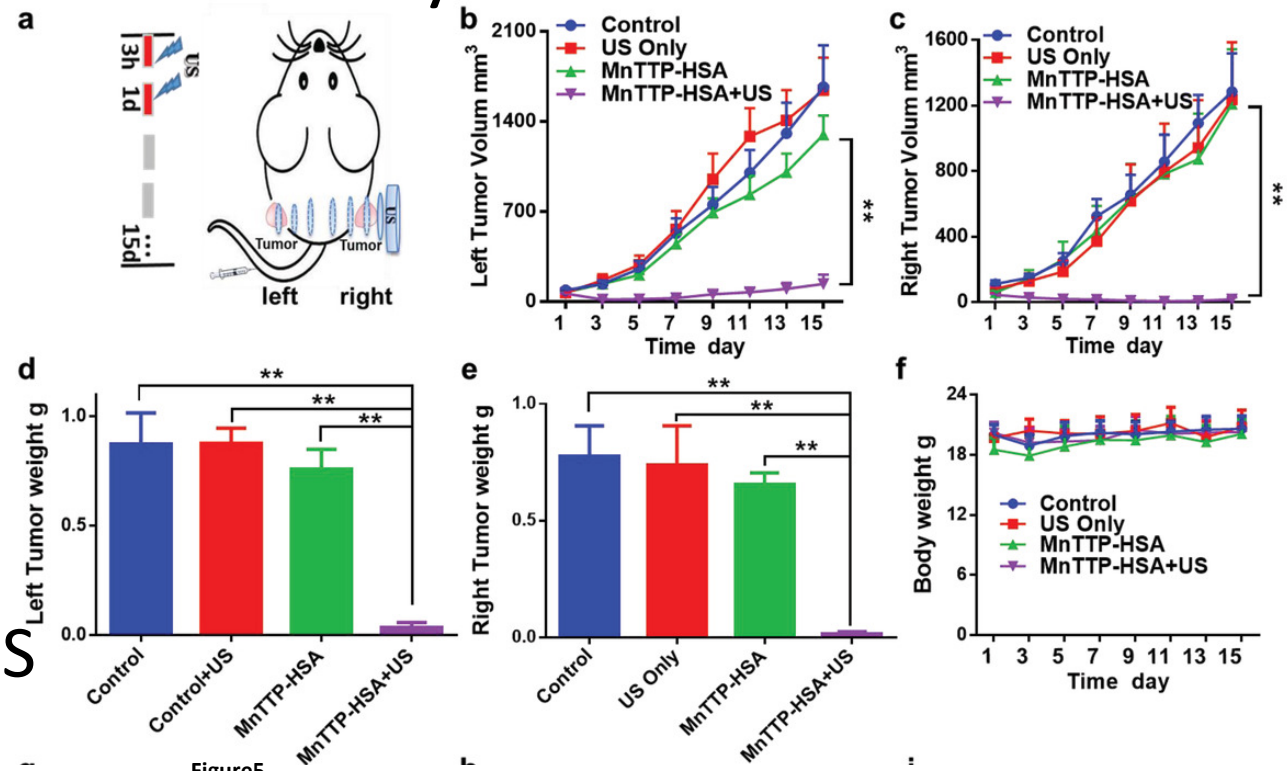

- MnTTP-HSA + US inhibited tumor growth of both side
- Good biosafety and biocompatibility

Figure5
In vivo SDT treatment efficiency of the MnTTP-HSA nanocomplex in nude mice bearing MCF-7 bilateral tumors. The mice were divided into control (untreated) group, US only group, MnTTP-HSA group, and MnTTP-HSA + US group. a) In vivo therapeutic protocol of SDT on MCF-7 tumor xenograft. The US probe was on the right tumor, and the ultrasound wave penetrated from right to left (1.0 MHz, 2 W cm^{-2}, 50% duty cycle, 5 min). The US irradiation was conducted twice at 3 and 24 h, respectively. b,c) MCF-7 tumor growth curves of left side and right side, respectively, with various treatments (**$p < 0.01$). d,e) The corresponding excised tumor weights of left and right side, respectively, acquired at the end of treatments (**$p < 0.01$). f) Body weights of the mice during the 15 d study period under the different conditions.

Ma, A. *et al.*, *Small*, **2019**, *15*, e1804028

Contents

Water-soluble Ir Complex

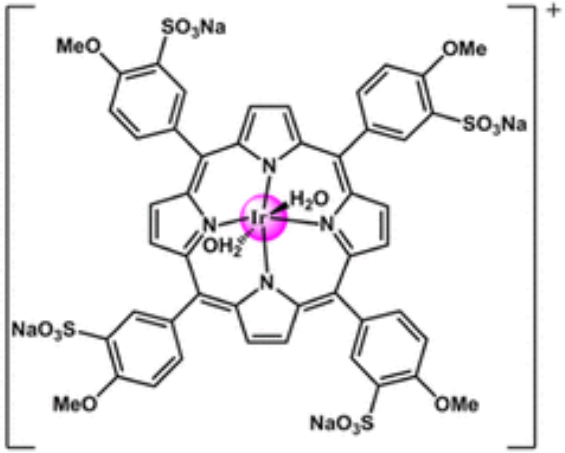

- Hydrophobic compounds
  - low saturation concentration
  - aggregate in the body fluid

⇩

- Porphyrin sulfonates are water-soluble
- IrTMPPS showed high water solubility
- HOMO/LUMO energy gap was 1.147 eV, easily excited by US

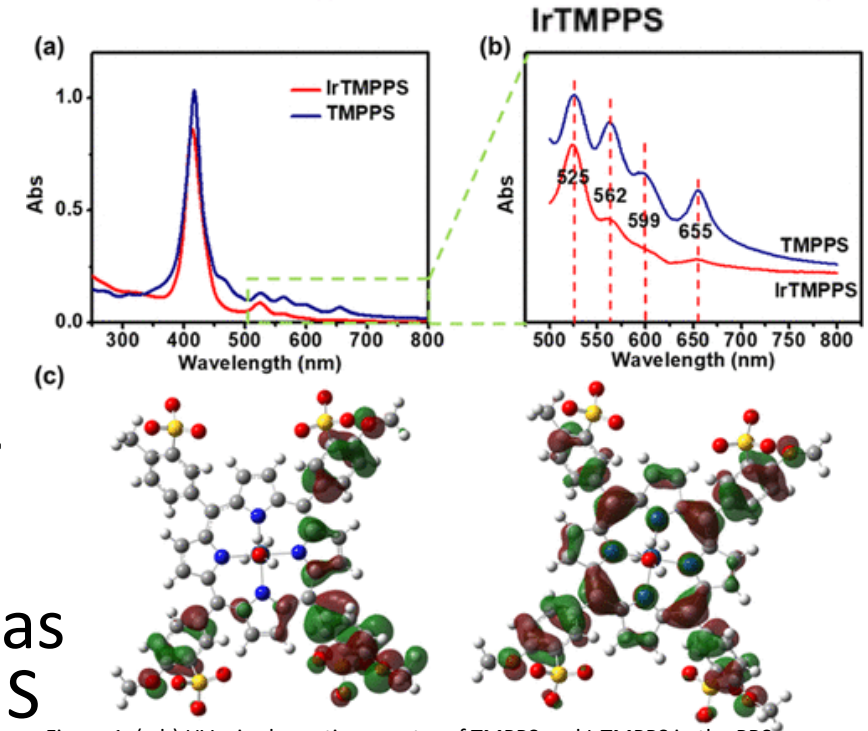

Figure 1. (a,b) UV–vis absorption spectra of TMPPS and IrTMPPS in the PBS solution. (c) HOMO–LUMO plots of IrTMPPS by DFT.

Xie, J. *et al., ACS Appl. Mater. Interfaces,* **2021**, *13*, 24, 27934–27944

$^1O_2$ Generation by IrTMPPS

- $^1O_2$ increased depending on US irradiation time
- DPA was oxidized constantly under US
- IrTMPPS had good sono-stability
- IrTMPPS produced $^1O_2$ but not ・OH after US irradiation

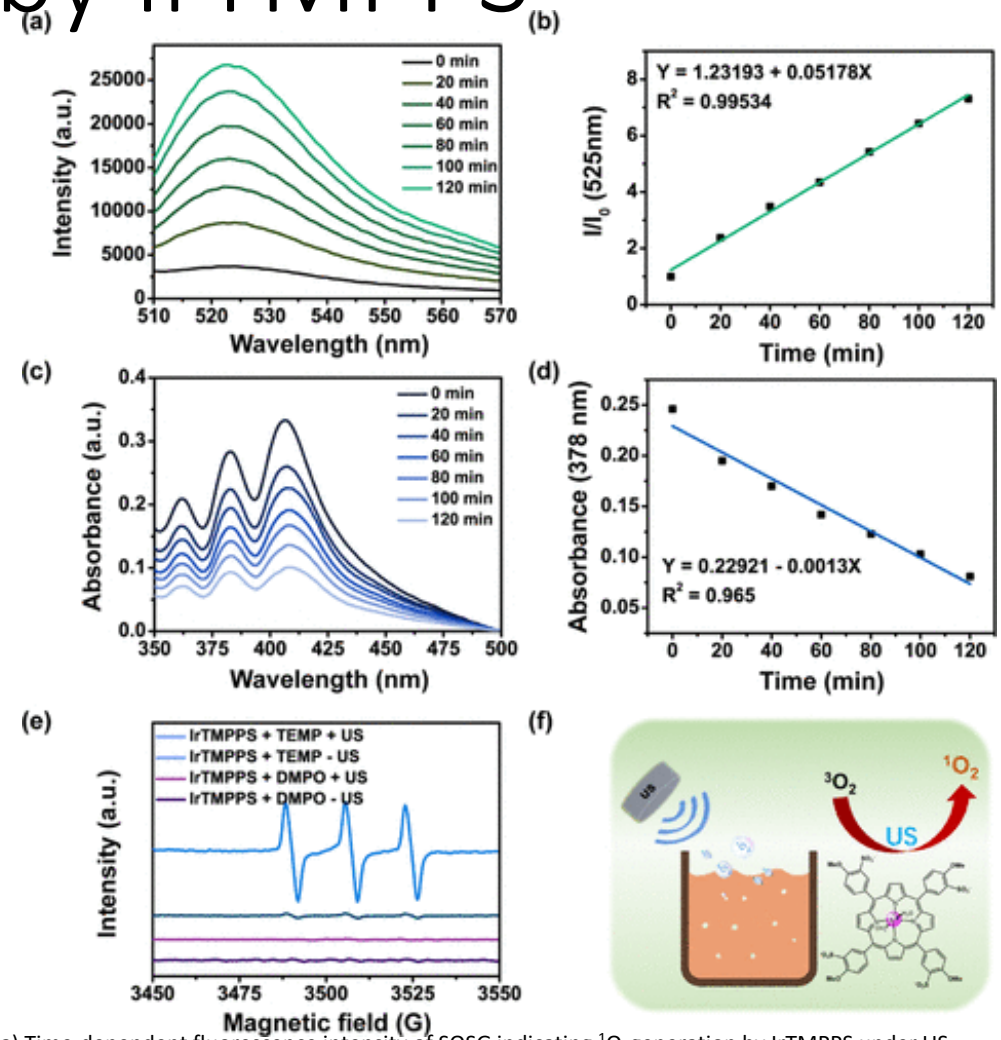

Figure 2. (a) Time-dependent fluorescence intensity of SOSG indicating $^1O_2$generation by IrTMPPS under US irradiation. (b) Rate constant for SOSG fluorescence intensity depending on US irradiation time in the presence of IrTMPPS. (c) Time-dependent absorption of DPA suggesting $^1O_2$ generation by IrTMPPS under US irradiation. (d) Rate constant for DPA absorption depending on the US irradiation time in the presence of IrTMPPS. (e) $^1O_2$ generation of IrTMPPS was demonstrated by ESR spectra. The power of US was 0.3 W cm^{-2}, 3.0 MHz. (f) Schematic illustration of $^1O_2$ generation by IrTMPPS under US irradiation.

Xie, J. *et al., ACS Appl. Mater. Interfaces,* **2021**, *13*, 24, 27934–27944

NADH Sonocatalytic oxidation

- NADH decreased and NAD^+ increased by IrTMPPS + US
- NADH oxidation was also monitored with ESR and NMR
- IrTMPPS consume NADH by US irradiation at the cellular level →destroyed redox balance induces cancer cell death

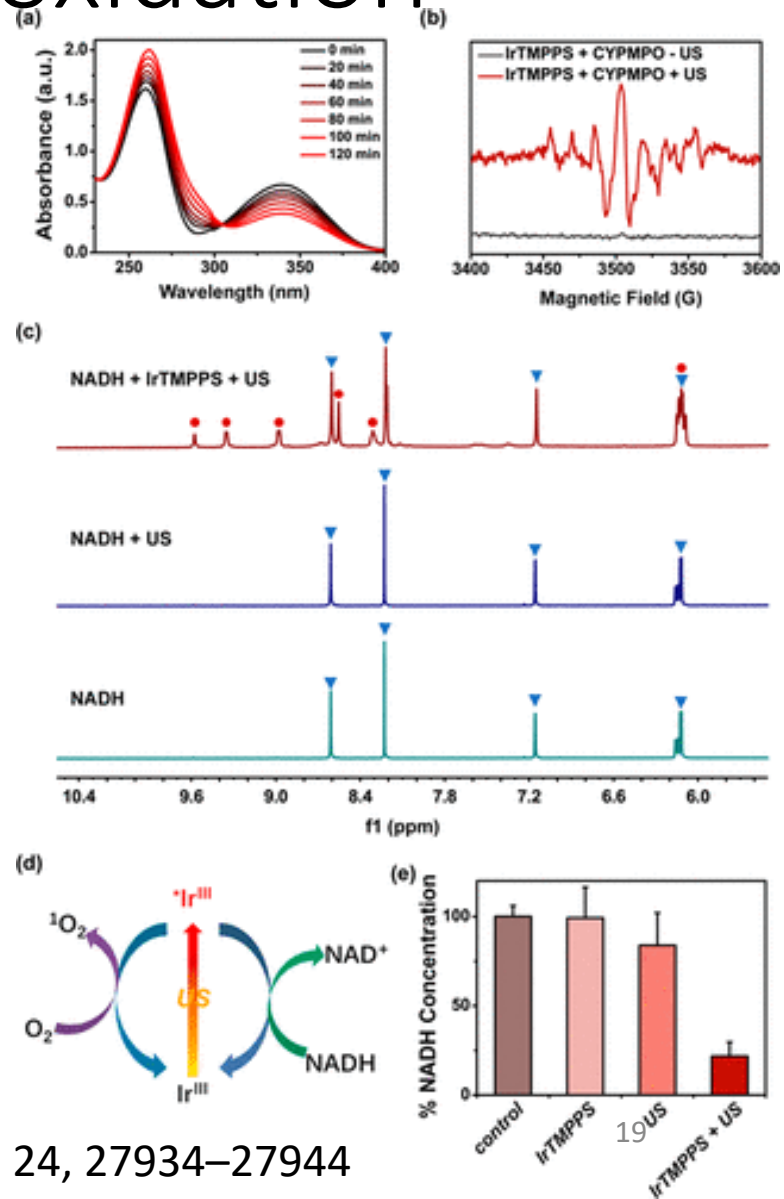

Figure 3. (a) Reaction of IrTMPPS and NADH in PBS solution under US irradiation detected by UV–vis spectra. (b) ESR spectra of $NAD^{\bullet}$ radicals trapped by CYPMPO demonstrating NADH oxidized by IrTMPPS under US irradiation. (c) Sonocatalytic oxidation of NADH (3.5 mM) by IrTMPPS (0.25 mM) without US or with US irradiation was monitored by ^1H NMR spectroscopy. Peaks classified with blue triangles represent NADH and red circles represent NAD^+. (d) Schematic illustration of IrTMPPS for sonocatalytic oxidation of NADH and generation of $^1O_2$. (e) NADH concentrations in the treated 4T1 cells. US irradiation: 3.0 MHz, 0.3 W cm^{-2}.

Xie, J. *et al., ACS Appl. Mater. Interfaces,* **2021**, *13*, 24, 27934–27944

Sono-toxicity of IrTMPPS *In Vitro*

- Appropriate US irradiation power was 0.3 W/cm^2 and irradiation time was 20 min.
- IC_{50} of IrTMPPS was 3.43 μM toward 4T1 cells
- IC_{50} toward other cancer cells were all below 10 μM
- With IrTMPPS and US, lots of cancer cells died

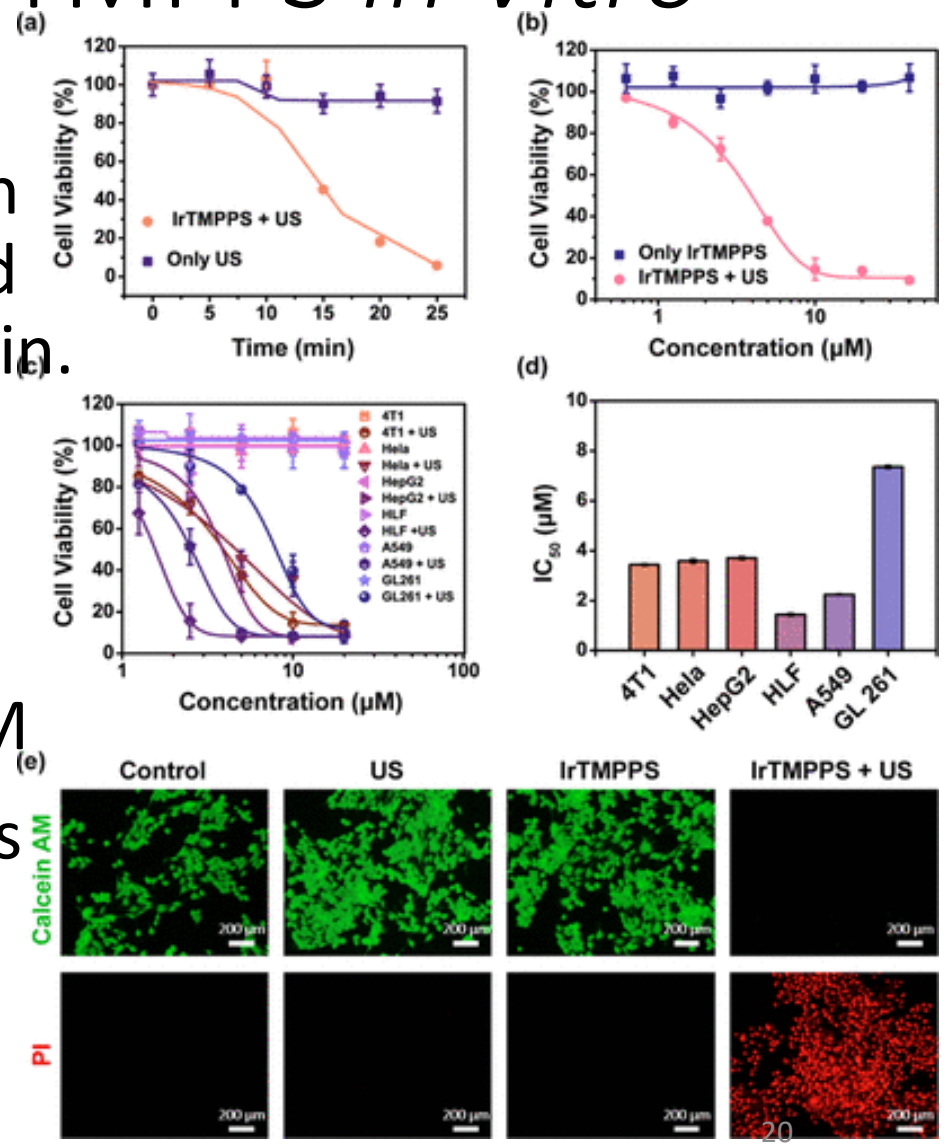

Figure 5. (a) Cell viabilities of 4T1 cells incubated with IrTMPPS (10 μM) under different US irradiation time. (b) Viability of 4T1 cells incubated with various concentrations of IrTMPPS under US irradiation for 20 min. (c) Cytotoxic effects of IrTMPPS on different types of cells with or without US irradiation. (d) Sono-toxicity (IC_{50}, μM) of IrTMPPS toward different types of cells. (e) Images of the living 4T1 cells co-stained with calcein AM (4 μM, 0.5 h) and propidium iodide (6 μM, 0.5 h) after different treatments. Calcein AM: λ_{ex} = 460 nm, λ_{em} = 540 ± 30 nm; PI: λ_{ex} = 540 nm, λ_{em} = 610 ± 30 nm.

Xie, J. *et al., ACS Appl. Mater. Interfaces,* **2021**, *13*, 24, 27934–27944

In Vivo SDT with IrTMPPS

- $^1O_2$ generated in deep tissue (>10 cm)
- Low selectivity →intratumoral injection
- Growth of tumors in mice treated with IrTMPPS + US was suppressed

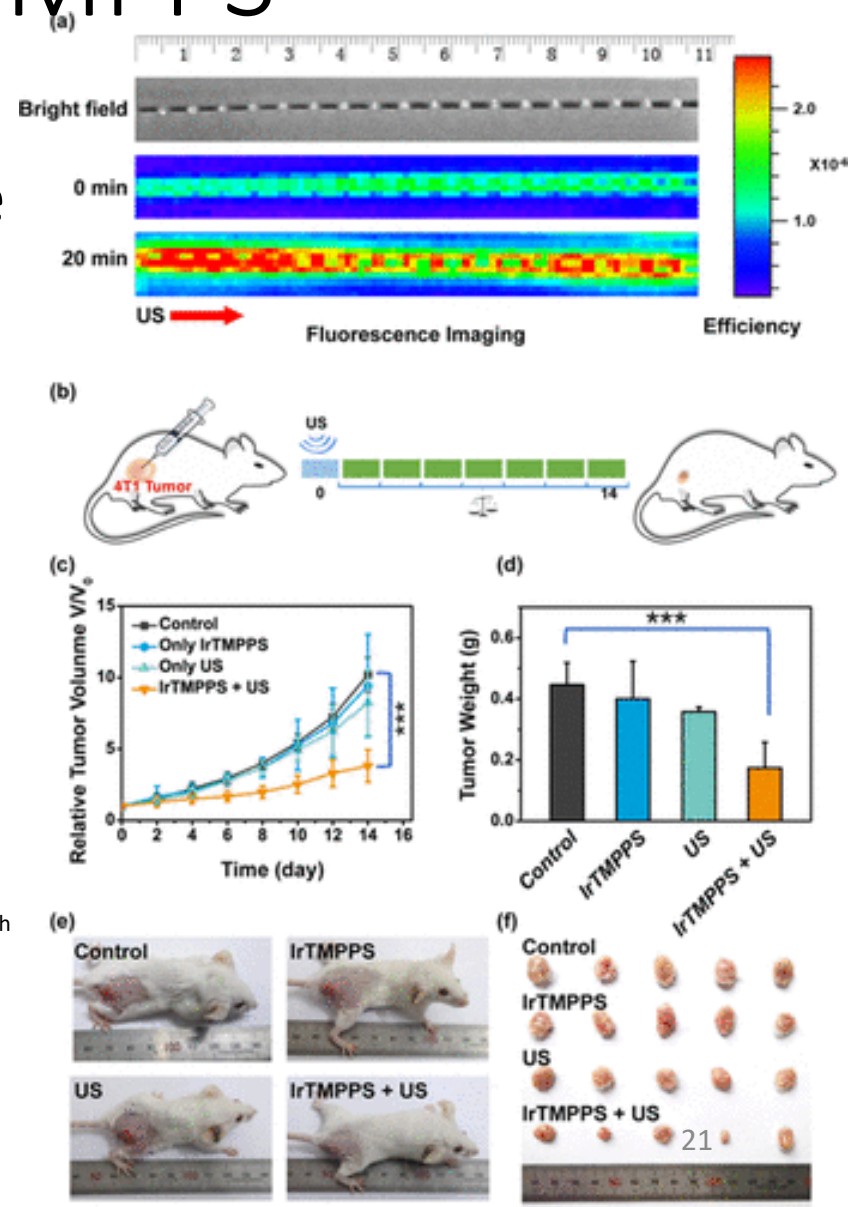

Figure 6. (a) Fluorescence imaging for investigating $^1O_2$ generation in the presence of IrTMPPS and SOSG probe in tissue-mimicking gel model (>10 cm) under 20 min US irradiation. SOSG and IrTMPPS mixing solution was injected in every hole. (b) Schematic of the *in vivo* therapeutic protocol for SDT. Mice were irradiated by US (0.3 W cm^{-2}, 3.0 MHz) for 20 min after i.t. injected with 25 μL of PBS containing 500 μM IrTMPPS. (c) Tumor growth curves after different treatments. Error bars were standard errors based on five mice per group. (d) Tumor weights of mice at day 14 after various treatments. (e) Representative images of mice at day 14 after different treatments. (f) Photos of tumors of mice at 14 day. ***$p < 0.001$.

Xie, J. *et al., ACS Appl. Mater. Interfaces,* **2021**, *13*, 24, 27934–27944

Anti-metastasis to Lungs

- Mice treated with IrTMPPS + US exhibited almost no lung metastasis sites
- IrTMPPS significantly inhibited tumor lung metastasis

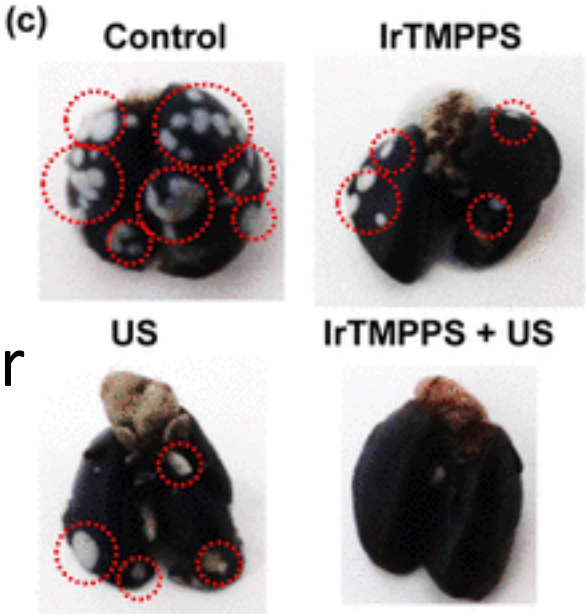

Figure 7. (c) Photos of India ink-stained lungs from mice at 40 days post various treatments. Spontaneous pulmonary breast cancer metastasis sites are pointed out by red circles.

Xie, J. *et al., ACS Appl. Mater. Interfaces,* **2021**, *13*, 24, 27934–27944

Short Summary

- SDT could treat deep-seated tumors.
- MnTTP-HSA presented the best SDT performance due to the lowest HOMO−LUMO gap energy
- SDT with IrTMPPS can suppress tumor growth and proliferation by generating $^1O_2$ and oxidizing NADH to NAD^+.

Contents

Pt-CuS Nanoparticles (PCPT)

- Photothermal Therapy (PTT)
  - Kill cancer cells with hyperthermia produced by light energy
- 808 nm laser + US

→Hyperthermia + $^1O_2$

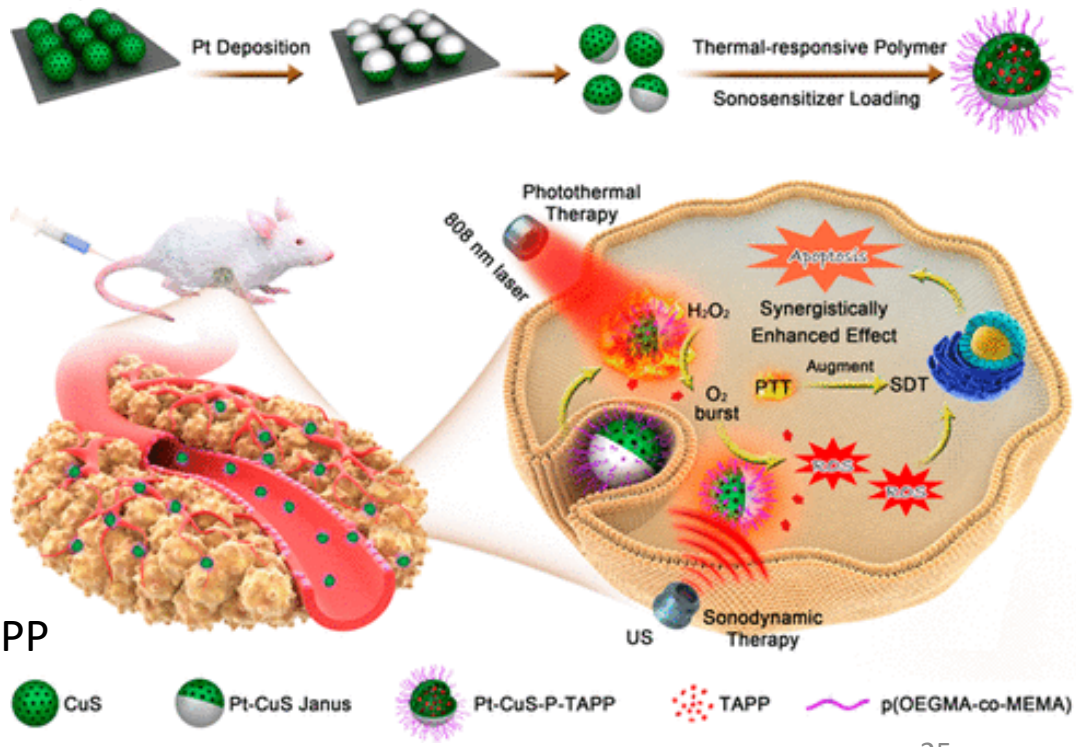

Pt: $H_2O_2 \rightarrow O_2$
TAPP: Sonosensitizer
Temperature-sensitive polymer
Increase biocompatibility
prevent premature release of TAPP

Liang, S. *et al., Nano Lett.* **2019**, *19*, 6, 4134–4145

Photothermal Effect of Pt-CuS in Solution

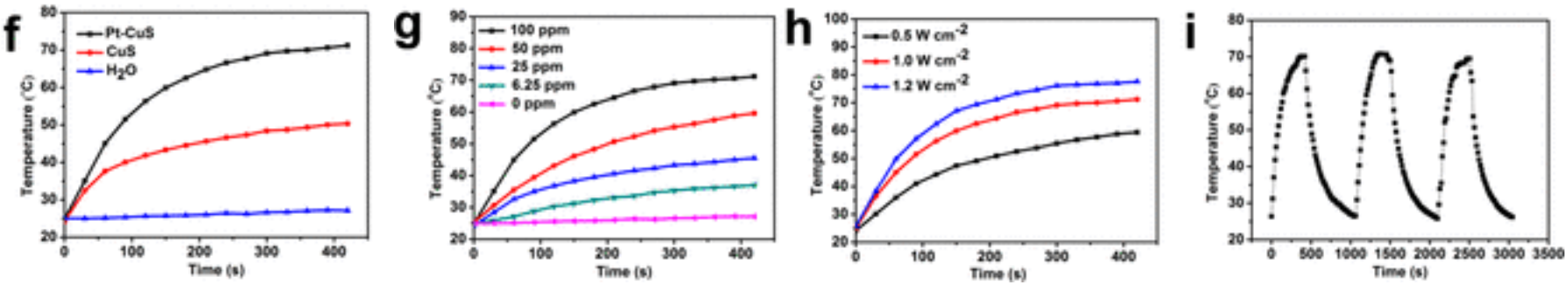

- Photothermal conversion efficiencies
  - Pt-CuS: 34.5%
  - CuS NPs: 23%
- Stable conversion ability

Figure2. (f) Temperature elevation curves of aqueous CuS and Pt-CuS solution with the same concentration of Cu (100 ppm) at 0.8 W cm^{-2} 808 nm laser irradiation for 420 s. (g) Temperature elevation curves of the aqueous Pt-CuS solution at various concentrations of Cu upon 0.8 W cm^{-2} 808 nm laser irradiation for 420 s. (h) Temperature elevation curves of the aqueous Pt-CuS solution (the concentration of Cu is 100 ppm) under 808 nm laser irradiation with various power densities for 7 min. (i) The photothermal stability of Pt-CuS solution (the concentration of Cu is 100 ppm) under 0.8 W cm^{-2} 808 nm laser irradiation.

Liang, S. *et al., Nano Lett.* **2019**, *19*, 6, 4134–4145

In Vitro ROS Generation by PCPT

- Catalase-like activity of Pt-CuS-P ($H_2O_2 \rightarrow O_2$)
- US exceeds light in $^1O_2$ generation

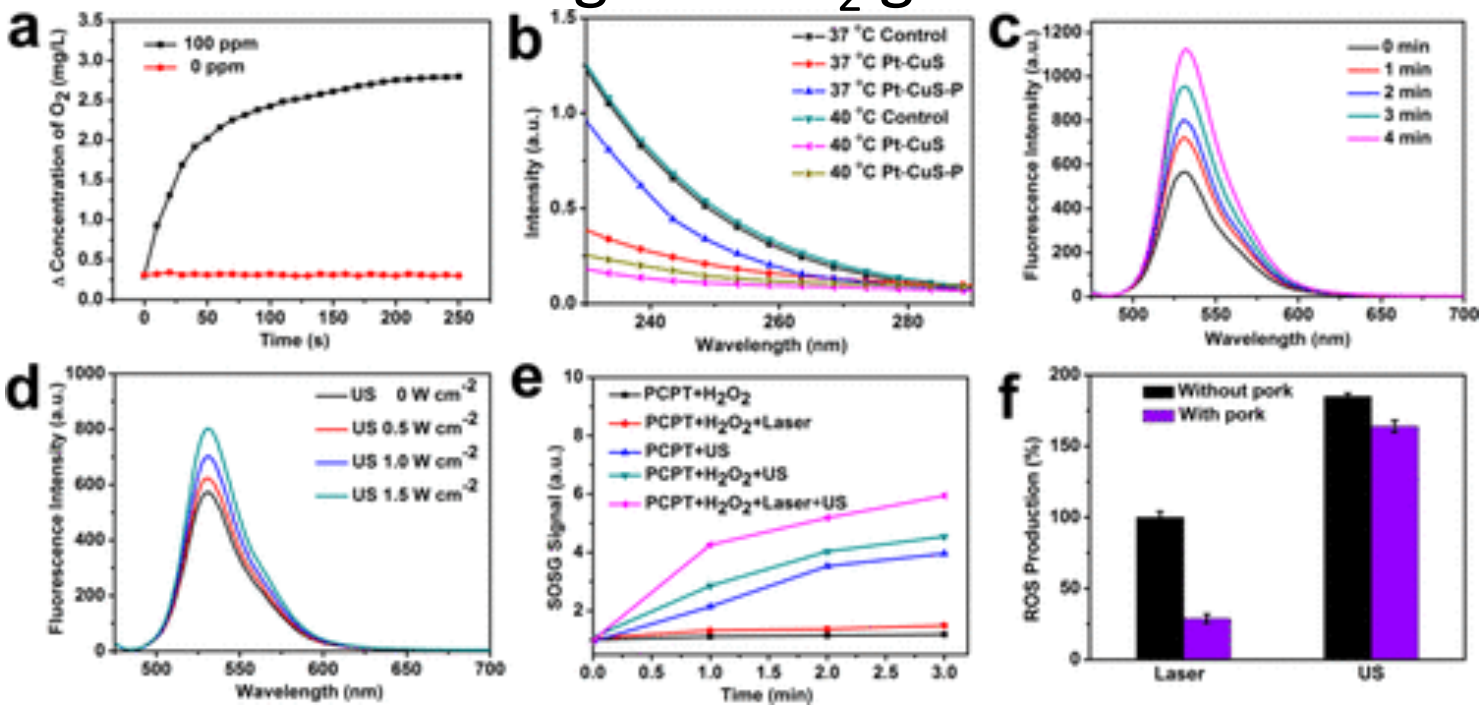

Figure 3. (a) The production of O_2 by Pt-CuS (100 ppm of Cu) in the concentration of 250 μM H_2O_2 in a N_2 environment. (b) UV–vis absorption spectrum of the remainder H_2O_2 after reaction with Pt-CuS and Pt-CuS-P at 37 and 40 ° C. (c) The fluorescence intensity of SOSG in the presence of PCPT with the concentration of 50 ppm upon US (1.0 MHz, 1.0 W cm^{-2}, 60% duty cycle) irradiation for fixed intervals durations. (d) The fluorescence intensity of SOSG in the presence of PCPT with the concentration of 50 ppm upon US irradiation at varied power densities. (e) The production of $^1O_2$ in the presence of PCPT (50 ppm) at different conditions. (f) Relative $^1O_2$ production from PCPT after 650 nm NIR light or US irradiation, with or without the screen of pork.

Liang, S. *et al., Nano Lett.* **2019**, *19*, 6, 4134–4145

In Vitro Cytotoxicity of PCPT

- PCPT entered the cytoplasmic vesicles
- PCPT + laser + US produced more ROS and enhanced anticancer effect
- SDT + PTT induced extensive apoptosis

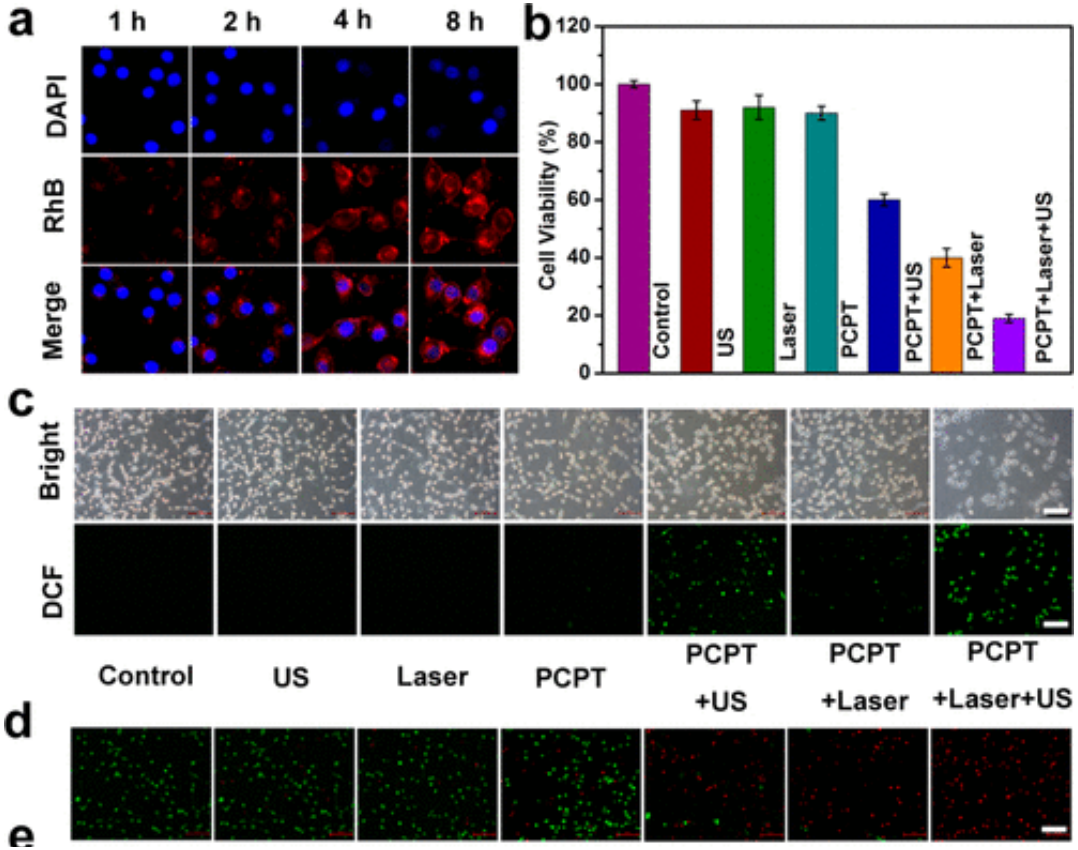

Figure 4. (a) Cellular endocytosis of PCPT by CT26 murine colon cancer cells at varied time points. (b) The viability of CT26 cells with different treatments, including control, only US, only laser, only PCPT, PCPT combined with US irradiation, PCPT combined with 808 nm laser irradiation, and PCPT combined with 808 nm laser and US irradiation. (c) Cellular production of $^1O_2$ with different treatments, including control, only US, only laser, only PCPT, PCPT combined with US irradiation, PCPT combined with 808 nm laser irradiation, and PCPT combined with 808 nm laser and US irradiation. (d) The fluorescence imaging of CT26 cells stained by calcein AM (green) and PI (red) after different treatments.

Liang, S. *et al., Nano Lett.* **2019**, *19*, 6, 4134–4145

In Vivo Tumor Inhibition Ability

- PCPT + US or Laser

  Inhibited tumor growth, but recurrence

- PCPT + US + Laser

  Eradicate tumor, no reoccurrence

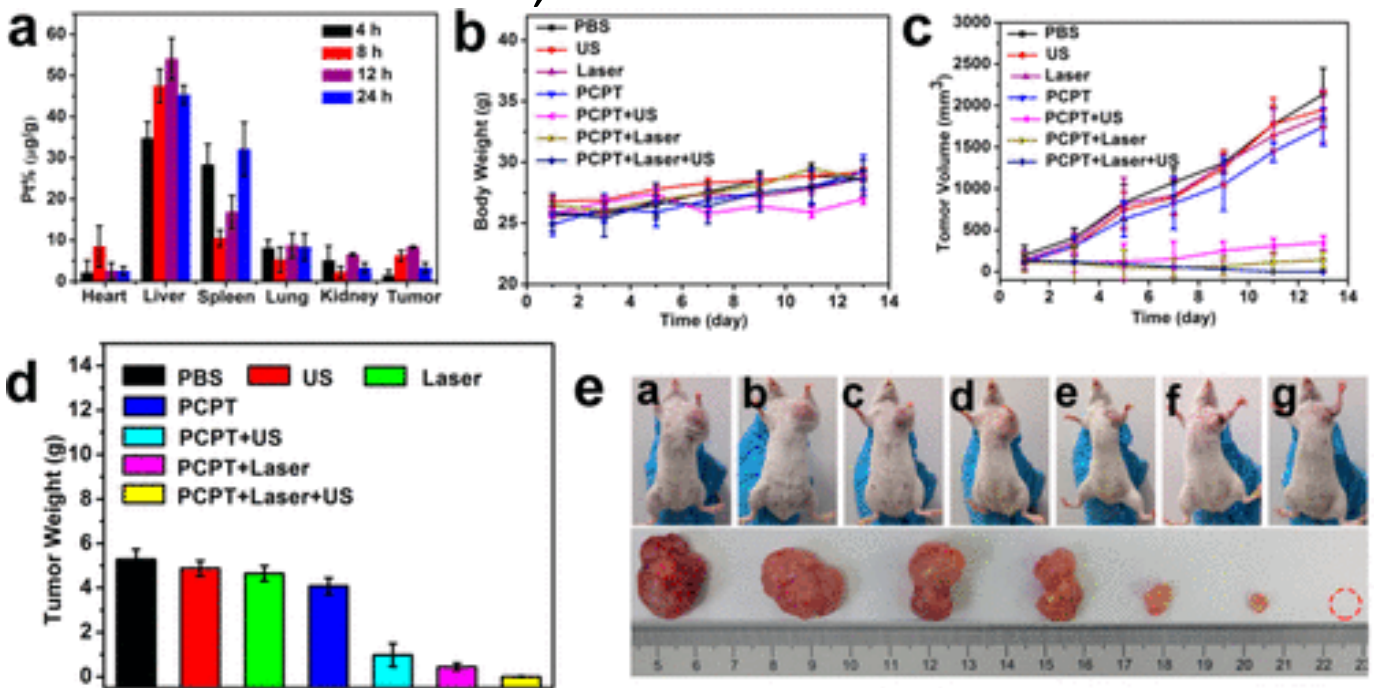

Figure 6. (a) Biodistribution of Pt in tumor and main organs after injection with PCPT intravenously for 4, 8, 12, and 24 h. (b) Body weight of CT26 tumor-bearing mice with different treatments during therapeutic duration. (c) Tumor volume change curves during therapeutic duration. (d) Tumor weights harvested by mice at the end of various treatments. (e) Representative digital photos of tumor-bearing mice after different therapies and digital photos of tumors from euthanized mice after different treatments for 13 days.

Liang, S. *et al.*, *Nano Lett.* **2019**, *19*, 6, 4134–4145

Contents

Summary

- SDT is a promising strategy for cancer treatment
- $^1O_2$ generation ability may be related to energy gap
- Solubility of sonosensitizer is important
- Combination of SDT and other methods can strengthen therapeutic effect

APPENDIX

In vitro SDT efficacy of MTTP-HSA

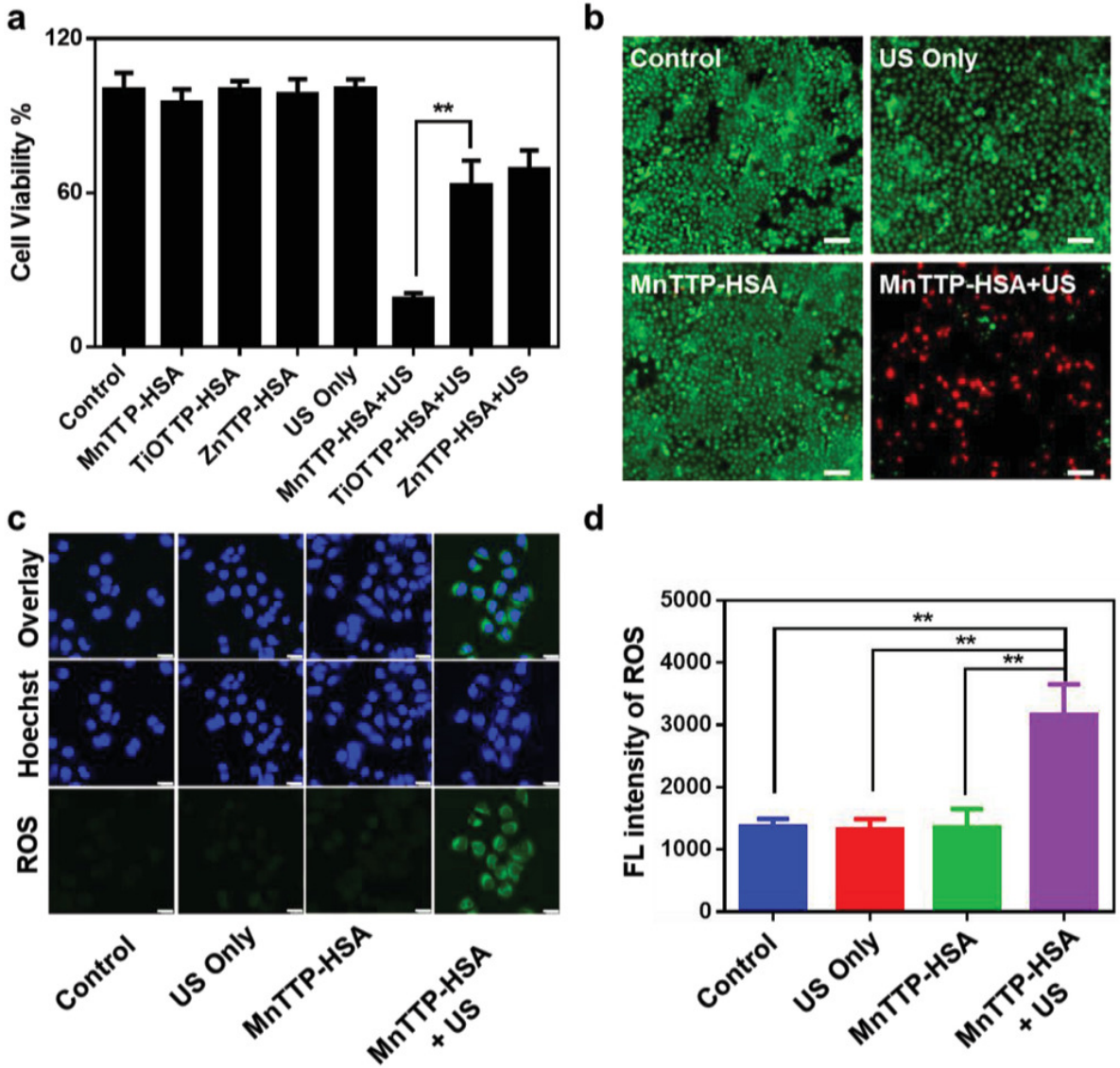

Figure3.
In vitro SDT efficacy of MTTP-HSA nanoparticles against MCF-7 cells. a) In vitro cytotoxicity of the three nanoparticles at identical concentrations (5.5 m) against MCF-7 cells after US irradiation (1 MHz, 2 W cm^{-2}, 3 min); the MnTTP-HSA showed the best inhibition to MCF-7 cells among the three nanoparticles (**$p < 0.01$). b) FL images of MCF-7 cells stained by calcein-AM and PI after various treatments; Viable cells were stained green with calcein-AM, and dead/later apoptosis cells were stained red with PI (scale bar = 100 µm). The MnTTP-HSA + US treatment clearly induced apoptosis/necrosis. c) CLSM images of ROS in MCF-7 cells strained by DCFH-DA after different treatments (scale bar = 25 µm); the MnTTP-HSA + US treatment produced a large quantity of ROS. d) The intracellular quantitation of ROS generation after different treatments. The intensity of the ROS signal was significantly higher in the MnTTP-HSA + US group than the others (**$p < 0.01$).

Ma, A. *et al.*, *Small*, **2019**, *15*, e1804028

MRI/PA Dual-Modal Imaging of the MnTTP-HSA

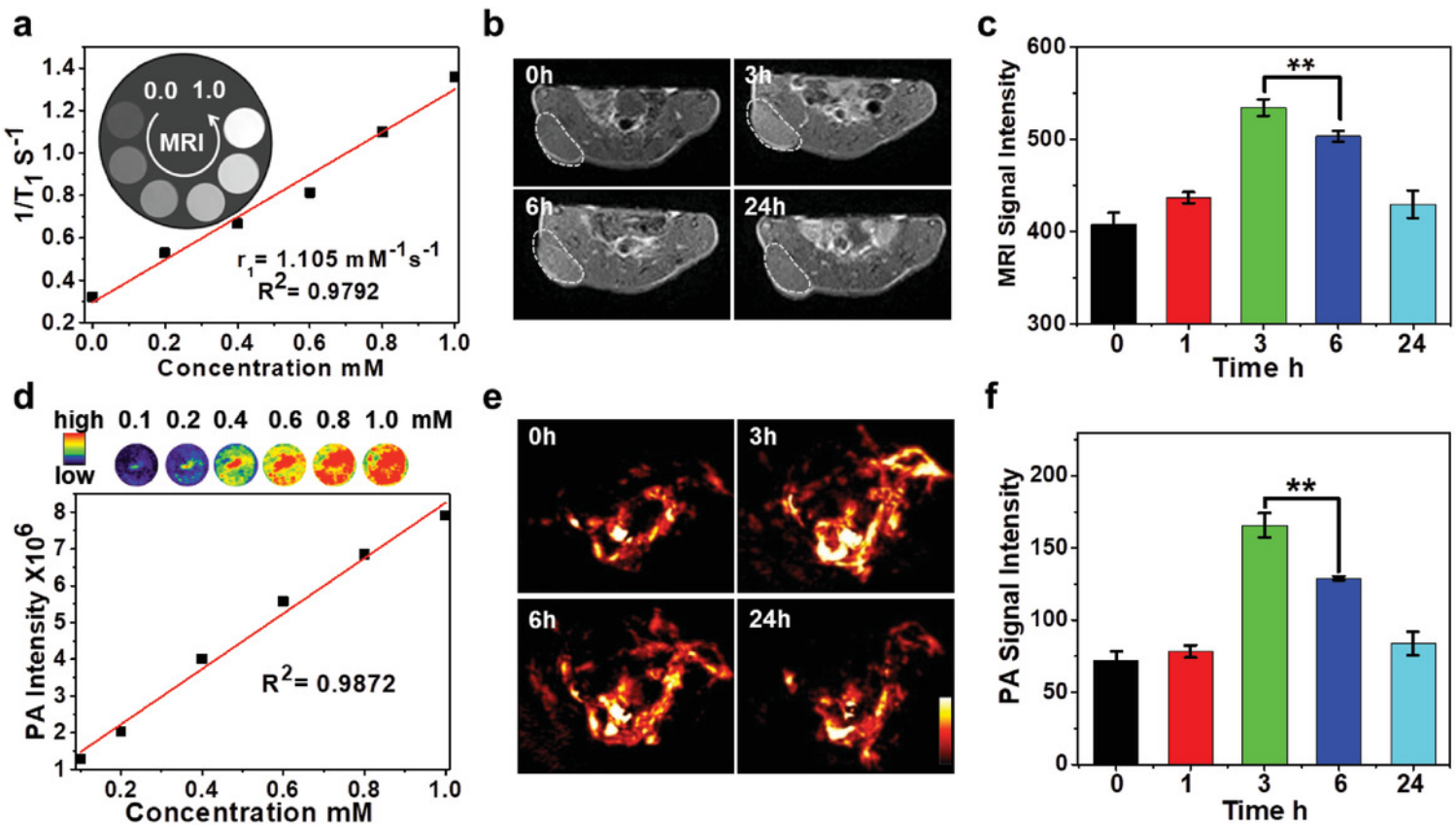

Ma, A. *et al.*, *Small*, **2019**, *15*, e1804028

Figure4. MR and PA imaging of the MnTTP-HSA nanocomplex. a) Longitudinal relaxation rates ($1/T_1$) versus the concentration of MnTTP-HSA (0, 0.2, 0.4, 0.6, 0.8, and 1.0 × 10^{-3} m); the inset was the T_1-weighted MR images of MnTTP-HSA aqueous solutions at varied concentrations. b) Time-dependent in vivo T_1-weighted MR images of MCF-7 tumor-bearing nude mice after the intravenous injection of MnTTP-HSA. c) Corresponding T_1-weighted MR signal intensity of MnTTP-HSA in tumor varying with time (**$p < 0.01$). d) Photoacoustic (PA) signal intensity versus the concentration of MnTTP-HSA (0.1, 0.2, 0.4, 0.6, 0.8, and 1.0 × 10^{-3} m); the inset was the PA images at various concentrations of MnTTP (λ_{ex} = 680 nm). e) Time-dependent PA images of MCF-7 solid tumors after the intravenous injection of MnTTP-HSA. f) The time-dependent PA signal intensity of MnTTP-HSA in tumor (**$p < 0.01$).

Intracellular Localization and ROS Generation

- IrTMPPS specifically targeted lysosomes of 4T1 cells.

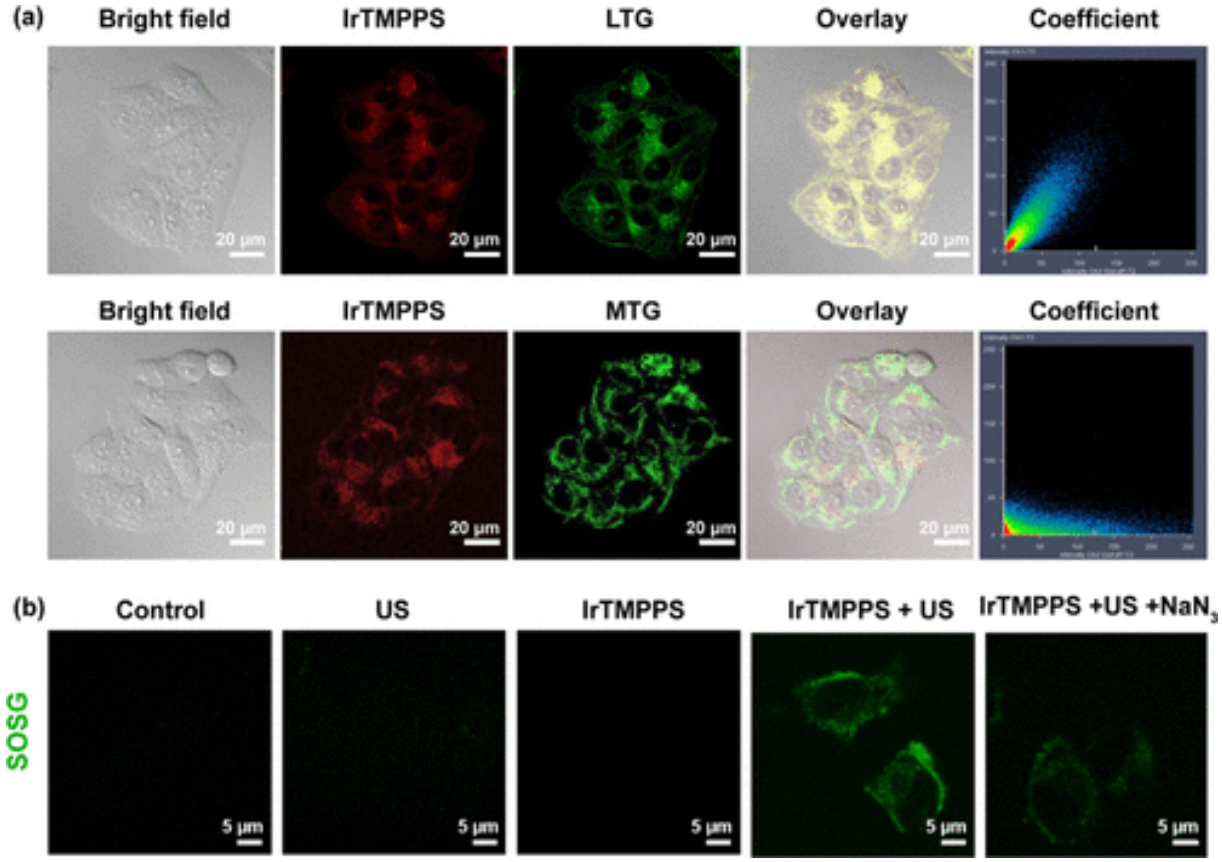

Figure 4. (a) Confocal microscopy images of the living cells treated with IrTMPPS (10 μM, 4 h) and co-stained with Lyso-Tracker Green (LTG, 5 μM, 45 min) or Mito Tracker Green (MTG, 200 nM, 45 min). IrTMPPS: λ_{ex} = 405 nm, λ_{em} = 695 ± 30; nm. MTG: λ_{ex} = 488 nm, λ_{em} = 516 ± 30 nm; LTG: λ_{ex} = 458 nm, λ_{em} = 505 ± 30 nm. (b) Confocal microscopy images of 4T1 cells treated with IrTMPPS (20 μM, 4 h) and co-stained with SOSG in the presence or absence of NaN_3 under different conditions. SOSG probe: λ_{ex} = 488 nm, λ_{em} = 525 ± 30 nm.

Xie, J. *et al., ACS Appl. Mater. Interfaces,* **2021**, *13*, 24, 27934–27944

In Vivo PA Imaging and Upregulation of Tumor Oxygenation

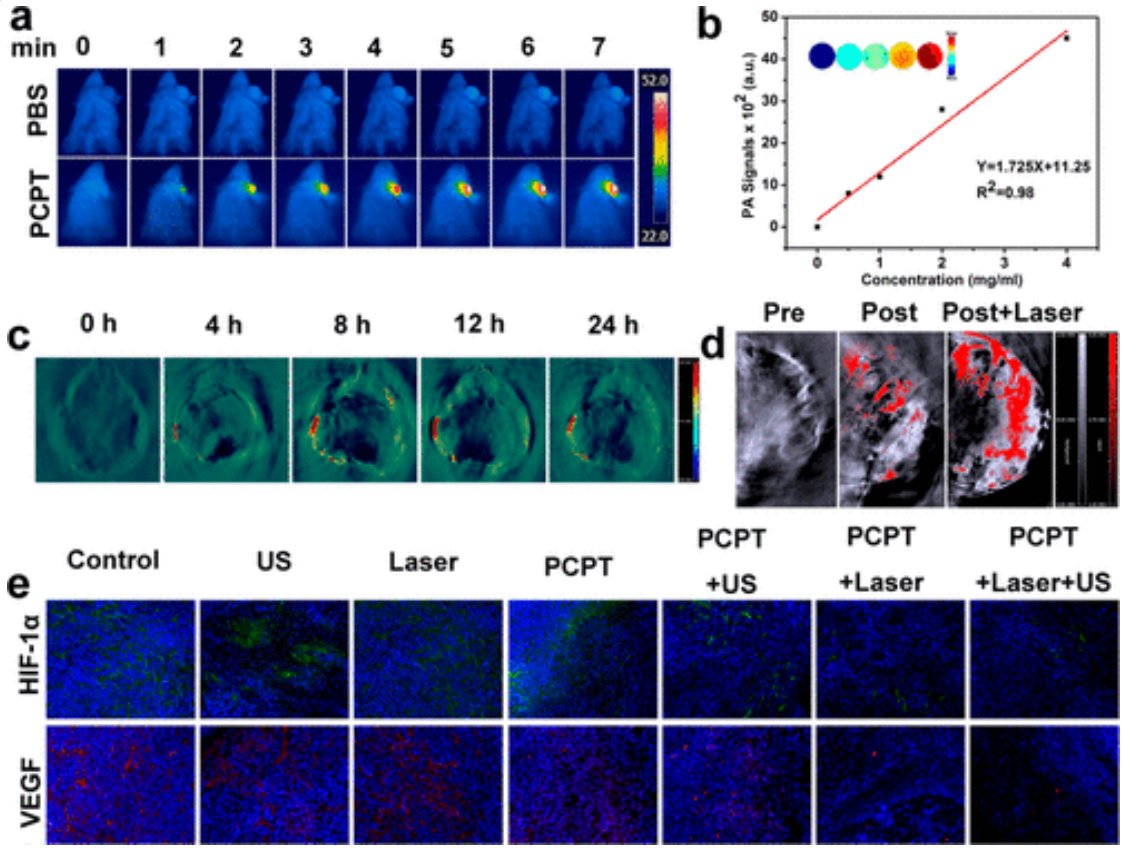

Figure 5. (a) *In vivo* NIR thermal imaging of CT26 tumor-bearing mice after intravenous injection of PCPT (20 mg kg^{-1}) for 12 h and combined with 808 nm laser irradiation. (b) *In vitro* PA imaging of different concentrations of Pt-CuS NPs. (c) *In vivo* PA imaging of the tumor-bearing mice intravenous injection with PCPT (20 mg kg^{-1}) at different times. (d) The blood oxygen saturation of tumors before and after intravenous injection with PCPT (20 mg kg^{-1}) and combined with 808 nm laser irradiation. (e) The representative immunofluorescence images of tumor slices after different treatments for 24 h. The nuclei were stained with DAPI (blue); hypoxia areas were stained with HIF-1α (green), and blood vessels were stained with VEGF (red).

Liang, S. *et al., Nano Lett.* **2019**, *19*, 6, 4134–4145